SPECIAL ISSUE PAPER

Implicit smoothed particle hydrodynamics model for simulating incompressible fluid-elastic coupling

Xiaokun Wang[1,2,3] | Tiancheng Wang[1] | Jiamin Wang[1] | Yanrui Xu[1] |
Xiaojuan Ban[1,4,5] | Houbin Huang[6] | Zhihong Zhu[7] | Jian Chang[3] | Jian Jun Zhang[3]

[1]School of Intelligence Science and Technology, University of Science and Technology Beijing, Beijing, China

[2]Beijing Key Laboratory of Knowledge Engineering for Materials Science, University of Science and Technology Beijing, Beijing, China

[3]National Centre for Computer Animation, Bournemouth University, Poole, UK

[4]Beijing Advanced Innovation Center for Materials Genome Engineering, University of Science and Technology Beijing, Beijing, China

[5]Key Laboratory of Perception and Control of Intelligent Bionic Unmanned Systems, Ministry of Education, University of Science and Technology Beijing, Beijing, China

[6]Chinese PLA General Hospital, Beijing, China

[7]Hainan Hospital of Chinese PLA General Hospital, Sanya, Hainan, China

Correspondence
Xiaojuan Ban, University of Science and Technology Beijing, Beijing, China.
Email: banxj@ustb.edu.cn

Jian Chang, National Centre for Computer Animation, Bournemouth University, Poole, UK.
Email: JChang@bournemouth.ac.uk

Funding information
Horizon 2020-Marie Skłodowska-Curie Action-Individual Fellowships, Grant/Award Number: 895941; Guangdong Basic and Applied Basic

Abstract

Fluid simulation has been one of the most critical topics in computer graphics for its capacity to produce visually realistic effects. The intricacy of fluid simulation manifests most with interacting dynamic elements. The coupling for such scenarios has always been challenging to manage due to the numerical instability arising from the coupling boundary between different elements. Therefore, we propose an implicit smoothed particle hydrodynamics fluid-elastic coupling approach to reduce the instability issue for fluid-fluid, fluid-elastic, and elastic-elastic coupling circumstances. By deriving the relationship between the universal pressure field with the incompressible attribute of the fluid, we apply the number density scheme to solve the pressure Poisson equation for both fluid and elastic material to avoid the density error for multi-material coupling and conserve the non-penetration condition for elastic objects interacting with fluid particles. Experiments show that our method can effectively handle the multiphase fluids simulation with elastic objects under various physical properties.

KEYWORDS
elastic simulation, fluid-solid coupling, multiple fluid interaction, particle systems, physically based animation

1 | INTRODUCTION

In daily life, most solid objects, like rubber, jelly, biological tissue and so forth are elastic. These elastomers often co-exist with fluidic substances simultaneously, such as blood flowing in blood vessels and lifebuoys floating on water, composing a complex fluid-elastic coupling scenario with multiple fluids and elastics interacting. Simulation of these complex scenes has always been a tough nut in computer graphics, especially for particle-based Lagrangian fluid simulation like smoothed particle hydrodynamics (SPH).

When dealing with the interactions of two objects with different densities, the numerical discontinuity that appears in the pressure field. Due to approximation error, the discontinuous pressure field hinders the simulation stability for traditional SPH computation procedures.[1,2] To address this issue, Solenthaler and Pajarola proposed the number density scheme[3] to eliminate the density approximation error for explicit pressure computation. This is achieved by analyzing the fluid of different phases separately. However, this method does not incorporate well with more efficient implicit pressure projection SPH approaches.[4-6] During the iteration process, implicit solvers minimize the absolute value of density deviation rather than the density ratio, which destabilizing the direct use of the number density scheme.

Moreover, incorporating incompressible elastic objects into implicit SPH fluids algorithms also suffers from instability. Peer et al.[7] developed an implicit SPH formulation for incompressible linearly elastic solids. They addressed that the maximum density ratio between different phases had been a significant limitation in their method. The method only works with a small ratio of one order of magnitude that not negatively affect the performance.

To perform stable fluid-fluid, fluid-elastic, and elastic-elastic simulations under high-density ratio using implicit pressure projection SPH solvers, in this article, we propose an incompressible number density based SPH (INDSPH) method. First, the linear relationship between number density compression and pressure is constructed. Second, a number density incompressible solver is designed to circumvent the calculation error caused by the multiphase flow's heterogeneous rest density field.

2 | RELATED WORK

2.1 | Physics-based fluid simulation

Physics-based fluid simulation methods are usually divided into three categories: Eulerian, Lagrangian and hybrid methods.[8] The SPH method, a Lagrangian method, simulates fluid by discretizing it into a set of particles.[1] Becker et al.[2] proposed a weakly compressible SPH (WCSPH) method based on the Tait equation to approximate the incompressible state of the fluid. To further enhance the incompressibility of fluid, a series of efficient implicit incompressible solvers[4-6] were subsequently proposed. Fluids of different phases have different physical properties, such as density. Interaction simulation of multiphase fluids is an interesting topic in computer graphics community. It is difficult to track the interface between immiscible multiphase fluids and correctly calculate the interaction forces at the interface. Solenthaler and Pajarola[3] adjusted the standard SPH equation using a number density method to resolve density discontinuities at the interface. Alduán et al.[9] applied the density contrast SPH formulation to the Position-based fluids method. They developed a new multiphase fluids simulation framework to achieve good visualization. In addition, there are mesh-based interface tracking methods to handle multiphase fluids. Li et al.[10] combined mesh-based tracking and distance-field surface reconstruction to avoid complex remeshing operations. This approach was extended for surface tracking of more than three phases.[11]

2.2 | Physics-based elastic simulation

Elastic simulation is of great importance in many fields, such as various elastic tissues in the biomedical field. There are many ways to simulate elastic materials. The mass spring model was introduced in the early days of physical simulation and is a commonly used deformable model based on kinetic principles.[12] Continuum mechanics methods use constitutive models to explain the complex mechanical behavior of elastic, including grid-based finite element methods[13,14] and material point methods (MPM),[15] as well as SPH methods in the meshless methods. Although meshless methods are slightly less efficient than mesh-based methods in simulating elastic solids, they are superior in terms of flexibility. Becker et al.[16] used shape matching to determine the deformation gradient using the corotational line elasticity and explicit time integration methods. Ganzenmüller[17] introduced correction forces to suppress the control mechanism of zero-energy mode to solve the problem of unstable strong local oscillation and the inability to return to the static state. Kugelstadt et al.[18] designed an operator splitting formulation compatible with SPH and proposed an implicit zero-energy mode control by minimizing the quadratic energy function to improve the simulation efficiency.

2.3 | Fluid-elastic multi-material coupling

Multi-material coupling requires consideration of the interaction between the fluid and the elastic. The fluid-solid boundary conditions need to be fully considered to prevent penetration artifact. Yang et al.[19] combined SPH and nonlinear finite elements to animate the real-time interaction of fluids and deformable solids. Yan et al.[20] proposed the coupling method of multiphase fluids and solids to simulate the interaction between deformable solids, granular materials and fluids. Chen et al.[21] presented a particle method based on moving the least square reproducing kernel. They used the phase field model to ensure mass conservation and realize the phase evolution of multiphase fluids. MPM combines the advantages of Lagrangian particle representation and Eulerian grid representation, which can effectively simulate fluid-solid coupling. However, this method cannot resolve the discontinuous tangential velocities at the multi-material interface, leading to numerical stickiness, which can be visually quite intrusive. To avoid this issue, Fang et al.[22] proposed a new ghost matrix operator splitting scheme for solving the coupling of nonlinear elastic solids with incompressible fluids. They also devised a new MPM formulation for the interface orthogonal cutting unit to strengthen the free slip boundary conditions properly.

3 | BASIS OF SPH METHOD

3.1 | Governing equations of fluid mechanics

In order to truly simulate the dynamic behavior of the fluid, mathematical models are needed to describe the physical phenomena and motion of the fluid. The continuity equation describes the relationship between the change rate of fluid density in Lagrangian coordinates and the divergence of the velocity field as:

$$\frac{D\rho}{Dt} = -\rho(\nabla \cdot \mathbf{v}), \tag{1}$$

where $D(\cdot)/Dt$ denotes material derivative and $\mathbf{v}$ is the fluid velocity, ρ is the density. The Navier–Stokes equation describes the momentum field of incompressible fluid as:

$$\rho\frac{D\mathbf{v}}{Dt} = -\nabla p + \mu\nabla^2\mathbf{v} + \rho\mathbf{g}, \tag{2}$$

where p is the pressure, μ is the dynamic viscosity coefficient, and $\mathbf{g}$ is the gravitational acceleration. Equation (2) describes that the momentum change rate for each fluid parcel is affected by pressure, viscous force, and gravity.

3.2 | SPH discretization

The SPH method discretizes the continuous medium into a set of particles and discretizes the physical field using these sampling points. Arbitrary physical value A in the simulation domain can be approximated as:

$$A(\mathbf{x}_i) = \sum_j A(\mathbf{x}_j) V_j W(\mathbf{x}_i - \mathbf{x}_j, h),$$ (3)

where $\mathbf{x}$ and V are the position and volume of the particle, respectively. W is the smoothing kernel (such as cubic spline function[6]), and h is the support radius. Equation (3) indicates that any physical field value A of the particle i located at $\mathbf{x}_i$ can be approximately obtained by calculating the weighted sum of the values $A(\mathbf{x}_j)$ of all neighboring particles j within the support radius h centered on i.

The density can then be derived using Equation (3), as:

$$\rho_i = \sum_j m_j W_{ij},$$ (4)

where m is the mass, W_{ij} is the abbreviation of $W(\mathbf{x}_i - \mathbf{x}_j, h)$. The second-order derivative of value A can be expressed as:

$$\nabla A_i = \sum_j A_j V_j \nabla W_{ij},$$ (5)

where A_i is the abbreviation of $A(\mathbf{x}_i)$. Equation (5) is used to obtain higher-order derivatives of physical field quantities in the SPH method.

3.3 | Numerical error of density approximation

When simulating the motion of multiphase fluid with a non-uniform rest density field, the mass of particles in different phases is different. The discrepancy of mass between adjacent particles causes errors of density approximation according to Equation (4), resulting in instability in fluid simulation.

This numerical error issue is illustrated on the first row of Figure 1. It has two types of fluid (phase 1 and 2) with different rest densities 100 and 1000 (kg/m^3), with orange and blue color, respectively. So the mass of particles (with the same volume) representing each phase (m_1 and m_2) follows $m_2 = 10m_1$. Despite the particles being evenly distributed in space without overlapping (presenting an incompressible state), the density approximated according to Equation (4) diverges significantly from the rest density near the interaction boundary of the two-phase fluid, resulting in narrow gaps due to excessive pressure.
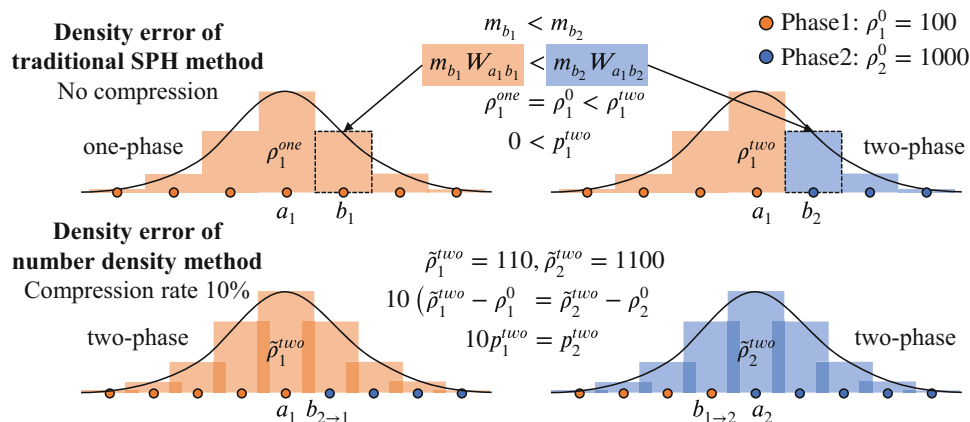

FIGURE 1 Schematic illustration of density calculation error.

Algorithm 1. INDSPH iterative solver

---

while $avg\left(\delta/\delta^0\right) > \eta$ **do**
    compute δ_i^{advec} (Equation 15)
    compute κ_i (Equation 18)
    compute $\mathbf{F}_i^p$ (Equation 19)
    update $\mathbf{v}_i^{\text{advec}}$ (Equation 20)
end while

To resolve the numerical error for the non-uniform rest density field, Solenthaler and Pajarola[3] used a number density scheme[23] to compute an adapted density, where the number density is calculated by:

$$\delta_i = \sum_j W_{ij}, \tag{6}$$

and the density calculated using Equation (4) is altered into an adapted density as:

$$\tilde{\rho}_i = m_i \delta_i. \tag{7}$$

When calculating the number density, Equation (6) sets the contribution of each neighbor particle j to be the same to avoid the error introduced in Equation (4). The adapted density in Equation (7) can be fitted into the explicit pressure method, but it can not be easily integrated with more efficient implicit pressure solvers like IISPH and DFSPH. As shown in the second row of Figure 1, when the compression occurs, the density compression value at the boundary of phase 2 is much higher than that of phase 1. Since the pressure value is computed from the density in implicit solvers, this can cause a large difference in the pressures of neighboring particles, which also leads to instability. This suggests that the interaction of high-density ratio multiphase fluids cannot be achieved using the adapted density method under the condition of Equation (7).

In conclusion, the existing implicit multiphase fluid methods cannot effectively handle the unstable pressure field issue when dealing with intense multiphase fluid interaction. In order to solve this problem, inspired by the DFSPH method,[6] we propose an incompressible number density based SPH algorithm to achieve the stable and efficient interaction effect between fluids with a high-density ratio. Based on the DFSPH method for single-phase fluid calculation, our method converts the pressure term generated by density compression into number density compression. The number density compression of each particle produced by the non-pressure term is offset by the pressure force. Therefore, the multiphase fluid interaction can be processed more accurately without additional computational overhead compared with the traditional DFSPH algorithm.

4 | INDSPH METHOD

Based on the existing implicit incompressible SPH method, we construct a simulation framework for the coupling of silicone oil and water, as shown in Figure 2. Aiming at minimizing the numerical error of the traditional SPH simulation method in dealing with a non-uniform rest density fluid field, we propose an incompressible number density based SPH model to ensure fluid incompressibility. The local equilibrium multiphase model[24] is applied to simulate the diffusion and emulsification effect between silicone oil and water. The implicit elastic SPH solver proposed by Peer et al.[7] is also incorporated into our framework and is integrated with our INDSPH method. We further introduce the surface tension model from Akinci et al.[25] (cohesion force and curvature force) into the framework to simulate the surface tension between two phases.

4.1 | Modification to SPH discretization

Instead of using density based pressure to negate the compression state in the traditional SPH method and former number density integration scheme, we use the number density to directly represent the compression state of the fluid. Our method
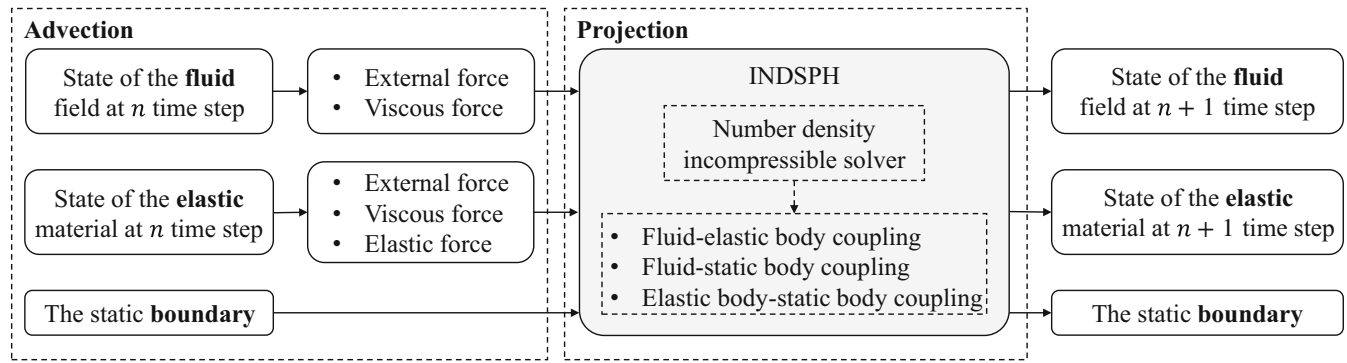
FIGURE 2 Incompressible coupling framework for the fluid, elastic body, and static boundary.

avoids the approximation error of the traditional SPH and improves the numerical accuracy of multiphase flow interaction without increasing the spatial and temporal computation complexity.

We propose to modify the SPH discretization to use the number density. According to Reference 3, The relationship $1/\delta_i = V_i$ holds, therefore based on Equation (3) the SPH discretization can be rewritten as:

$$A_i = \sum_j \frac{A_j}{\delta_j} W_{ij}; \tag{8}$$

and the gradient estimation becomes:

$$\nabla A_i = \sum_j \frac{A_j}{\delta_j} \nabla W_{ij}. \tag{9}$$

4.2 | Number density incompressible solver

Similar to the relationship between density compression and pressure in the traditional DFSPH method, a stiffness coefficient κ_i is used to establish the relationship between the number density compression state and pressure:

$$\nabla p_i = \kappa_i \nabla \delta_i = \kappa_i \sum_j \nabla W_{ij}. \tag{10}$$

According to the Navier–Stokes equation, the pressure force $\mathbf{F}_i^{p_i}$ exerted by pressure p_i on particle i can be expressed as:

$$\mathbf{F}_i^{p_i} = -\frac{m_i}{\rho_i} \nabla p_i = -\frac{\kappa_i}{\delta_i} \sum_j \nabla W_{ij}. \tag{11}$$

According to Newton's second law, the force exerted by pressure p_i on particle j should be exactly the opposite of that on particle i. According to Equation (11):

$$\mathbf{F}_j^{p_i} = \frac{\kappa_i}{\delta_i} \nabla W_{ij}. \tag{12}$$

The non-pressure force $\mathbf{F}_i^{\text{advec}}$ in the Navier–Stokes equation, which is the sum of external forces such as gravity, viscous force, and surface tension, is used to predict the advection velocity $\mathbf{v}_i^{\text{advec}}$:

$$\mathbf{v}_i^{\text{advec}} = \mathbf{v}_i + \Delta t \mathbf{F}_i^{\text{advec}} / m_i, \tag{13}$$

where Δt is the length of the time step.

The relationship between the material derivative of number density and velocity can be established as follows:

$$\frac{D\delta_i}{Dt} = -\delta_i \nabla \cdot \mathbf{v}_i = -\nabla \cdot (\delta_i \mathbf{v}_i) + \mathbf{v}_i \cdot \nabla \delta_i = \sum_j \left(\mathbf{v}_i - \mathbf{v}_j \right) \cdot \nabla W_{ij}. \tag{14}$$

From Equation (14), an intermediate number density can be obtained which only considers the effects of the advection velocity induced by the advection force:

$$\delta_i^{\text{advec}} = \delta_i - \delta_i \Delta t \nabla \cdot \mathbf{v}_i^{\text{advec}}. \tag{15}$$

The pressure is then solved to correct the compression in the intermediate number density so that the fluid remains in an incompressible state. To evaluate the compression state of number density, a rest number density is introduced as:

$$\delta_i^0 = \frac{1}{V_i^0}. \tag{16}$$

Since the velocity change of i induced by pressure p_i can be expressed as $\mathbf{v}_i^{p_i} = \Delta t \mathbf{F}_i^{p_i}/m_i$, the change of number density caused by pressure can be accordingly expressed using Equation (14):

$$\Delta \delta_i^p = \Delta t \sum_j \left(\mathbf{v}_i^{p_i} - \mathbf{v}_j^{p_i} \right) \cdot \nabla W_{ij} = \Delta t^2 \sum_j \left(\frac{\mathbf{F}_i^{p_i}}{m_i} - \frac{\mathbf{F}_j^{p_i}}{m_j} \right) \cdot \nabla W_{ij} = -\Delta t \frac{\kappa_i}{\delta_i} \left(\underbrace{\frac{\left(\sum_j \nabla W_{ij} \right)^2}{m_i}}_{d_i^{p_i}} + \underbrace{\frac{\sum_j \nabla W_{ij}^2}{m_j}}_{d_j^{p_i}} \right). \tag{17}$$

In order to make particle i incompressible, the change of number density due to non-pressure and pressure force must fulfill $\Delta \delta_i^p + \delta_i^{\text{advec}} = \delta_i^0$. Taking Equation (17) in it, we can obtain the description of κ as:

$$\kappa_i = \frac{\delta_i \left(\delta_i^{\text{advec}} - \delta_i^0 \right)}{\Delta t \left(d_i^{p_i} + d_j^{p_i} \right)}. \tag{18}$$

The total pressure force on i, which is the combination of forces induced by p_i and all p_j, is then computed as:

$$\mathbf{F}_i^p = \mathbf{F}_i^{p_i} + \sum_j \mathbf{F}_i^{p_j} = -\frac{\kappa_i}{\delta_i} \sum_j \nabla W_{ij} - \sum_j \frac{\kappa_j}{\delta_j} \nabla W_{ij}. \tag{19}$$

Then, the velocity change of the particle due to pressure is computed with $\mathbf{v}_i^p = \Delta t \mathbf{F}_i^p/m_i$, and the advection velocity is updated to be used in the next iteration:

$$\mathbf{v}_i^{\text{advec}} + = \Delta \mathbf{v}_i^p. \tag{20}$$

The advection velocity is iteratively updated as illustrated in Algorithm 1, until the global compression state of number density meets the standard (η is smaller than a threshold). η in Algorithm 1 is set as 1×10^{-4} in this article.

4.3 | Boundary condition

To handle the coupling boundary of fluid-rigid, fluid-elastic, and rigid-elastic, we classify particles representing those materials into static particles and dynamic particles. Static particles are the particles that do not move at all (i.e., stationary rigid particles) and are denoted as $\hat{i}$ and $\hat{j}$. Dynamic particles are the particles that can be moved by force, including fluid particles, two-way coupled rigid particles, and particles in elastic objects, which are denoted as $\tilde{\zeta}$ and $\tilde{j}$.

Since static particles cannot be moved by the pressure force, $d_i^{p_i}$, $d_i^{p_j}$, and $d_i^{p_j}$ are zero for all stationary particles $\hat{i}$. Thus, for static particles $\hat{i}$, Equation (17) is changed to:

$$\Delta \delta_{\hat{i}}^p = -\Delta t \kappa_{\hat{i}} d_j^{p_{\hat{i}}};$$ (21)

and for dynamic particles $\tilde{\zeta}$, Equation (17) is changed to:

$$\Delta \delta_{\tilde{\zeta}}^p = -\Delta t \kappa_{\tilde{\zeta}} \left(d_{\tilde{\zeta}}^{p_{\tilde{\zeta}}} + d_j^{p_{\tilde{\zeta}}} \right).$$ (22)

5 | EXPERIMENTS AND RESULTS

To verify the effectiveness of our method, we first simulate the dam break of two-phase fluid(see Figure 3) and the coupling of multiple elastic bodies(see Figure 5) respectively. Then we conduct coupling experiments between fluid (single-phase fluid and two-phase fluid) and three elastic objects (see Figures 6 and 8). Finally, for medical visualization applications, we carry out an elastic deformation experiment to simulate how biomechanical properties and intraocular cavity shape can affect tamponade results (see Figures 9 and 10). Our simulation algorithm is based on C++ coding, using eigen as a mathematical calculation tool. For visualization, Blender is used for offline animation rendering. We apply the surface reconstruction method proposed by Wang et al.[26] to generate fluid surfaces. We use a 128 GB memory workstation with two 16-core CPUs and a dominant frequency of 2.30 GHz to simulate all experiments.

5.1 | Multiphase fluid

We first conduct a violent two-phase fluid dam break experiment, as shown in Figure 3. The number density method fails to remain stable at a density ratio of 3, while our method can achieve a maximum density ratio of 75. Although the DFSPH can also simulate multiphase flow with a density ratio of 75, there is a large gap between the two phases. Comparing the change in compression ratio with simulation time(see Figure 4), we can see that the compression ratio of the DFSPH method fluctuates wildly.
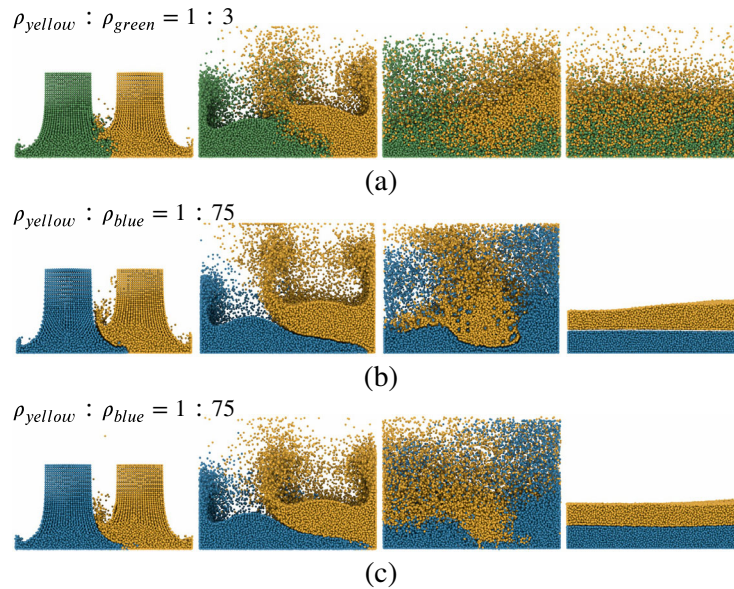

FIGURE 3 High-density ratio two-phase fluid interaction. Comparison of the maximum density ratio that can be simulated by (b) DFSPH, (a) number density and (c) our method.
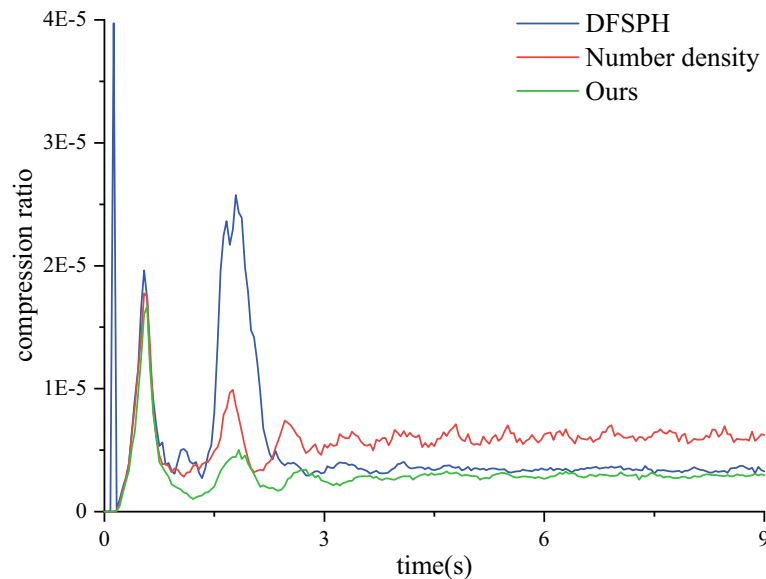
FIGURE 4 Comparison of compression ratio between the DFSPH method, the number density method and our method.

From Figure 4, we can see that the traditional DFSPH method suffers more from the compressibility despite the intense, unrealistic pressure energy generated between the two phases. On the contrary, our method can always maintain the lowest compression rate throughout the simulation process.

5.2 | Elastic-elastic coupling

The scenario in Figure 5 proves that our method is also suitable for elastic body coupling. Young's modulus used in the number density method is 200 KPa, and Young's modulus used in DFSPH and our method is 500 KPa. Both DFSPH and our method can achieve a maximum density ratio of 60, while the number density method can only achieve 5. We visualized the magnitude of the elastic force. The number density method shows the non-uniform color of particles at the phase interface, indicating a particle jitter problem. In the DFSPH method, the color of some particles at the interface is exceptionally dark (denoting powerful forces are applied on them) and discontinuous when the upper elastic cuboid falls to the lowest point. The cuboid tends to be unstable, with the color of internal particles being messy (middle column of Figure 5). In our method, the color of particles is darker at the interface and extended down along the boundary. In contrast, the middle color is lighter, which shows that our method is more continuous and robust to force conduction.

5.3 | Single phase fluid and elastic object coupling

We demonstrate the effect of fluid and elastic object coupling and compare it with the other two methods, as shown in Figure 6. The density ratio is $\rho_{red} : \rho_{purple} : \rho_{green} : \rho_{blue} = 1 : 2 : 3 : 4$. Because of the difference in density of these elastic objects, they are at different heights of the fluid when the scene reaches a stable state as Figure 6b–d shows. Due to pressure error, the DFSPH method produces a gap between the interface of the elastic object and the blue fluid phase. The number density method produces a boiling effect between the interfaces. Our method creates no gaps between the interfaces and is more stable.

Figure 7 shows the comparison of the cumulative iterations of the pressure solver between the DFSPH method, the number density method (with DFSPH) and our INDSPH method in this scenario. The number of iterations using our method is lower than DFSPH and the number density method, indicating an improvement in efficiency over the other two methods, especially when the fluid moves most violently.
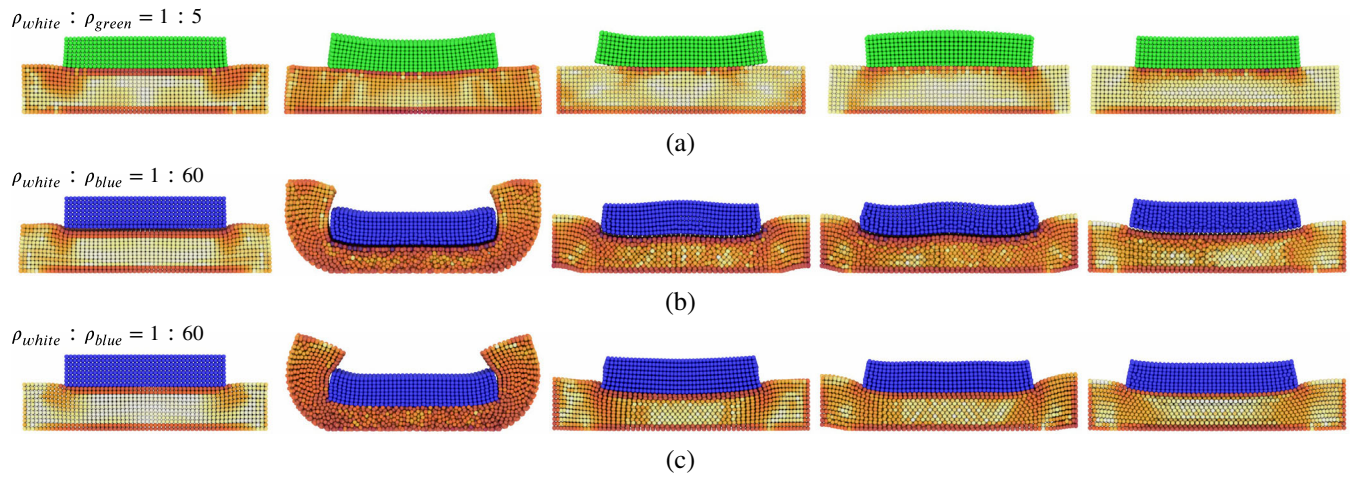
$\rho_{white} : \rho_{green} = 1 : 5$

$\rho_{white} : \rho_{blue} = 1 : 60$

$\rho_{white} : \rho_{blue} = 1 : 60$

(a)

(b)

(c)

FIGURE 5 An elastic cuboid falls onto another elastic cuboid. The depth of the bottom cuboid particle color indicates the degree to which the elastic resists deformation. (a) Number density; (b) DFSPH, (c) ours.
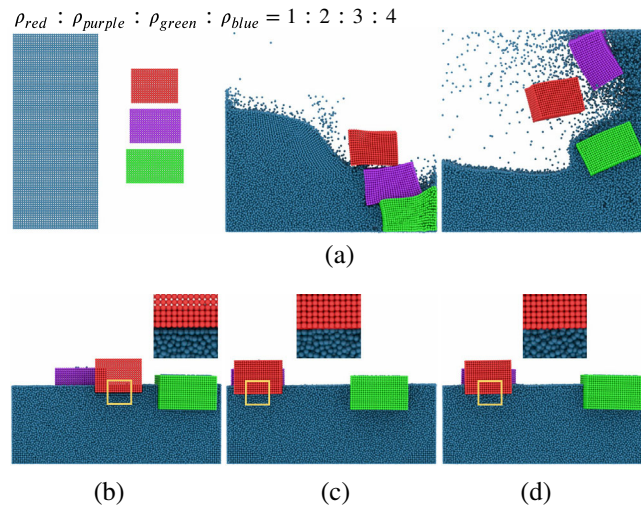
$\rho_{red} : \rho_{purple} : \rho_{green} : \rho_{blue} = 1 : 2 : 3 : 4$

(a)

(b)   (c)   (d)

FIGURE 6 Coupling of single phase fluid with elastic objects. The experiment is displayed in cross-section. (a) Simulation process; (b–d) Effects of different methods after reaching the steady state. (b) DFSPH; (c) number density; (d) ours.
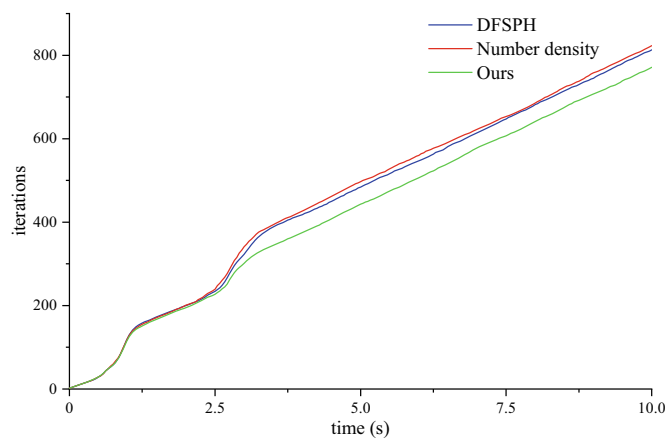
FIGURE 7 Comparison of iterations between the DFSPH method, the number density method and our method.

5.4 | Multiphase fluid and elastic object coupling

In this section, the experiment is conducted to verify the performance of the INDSPH method in simulating two-phase fluid coupling and the coupling with elastic objects.

The experiment is shown in Figure 8, where two fluid phases colored yellow and blue interact with three elastic objects, with the density ratio of: $\rho_{red} : \rho_{yellow} : \rho_{purple} : \rho_{blue} : \rho_{green} = 1 : 2 : 3 : 4 : 6$.

Figure 8a shows the simulation process, where the fluid blocks fall down and clash with the elastic objects. Figure 8b shows the condition of the experiment using the DFSPH method. Figure 8c shows the condition using the number density method by enforcing the incompressibility of the adapted density. Figure 8d shows the condition using the INDSPH method proposed in this article. By comparing the simulation results of the three methods, it can be seen that while exactly half of the red elastic object should be submerged in the yellow fluid because its density is half of the fluid's, the red object under the condition of DFSPH density computation is only submerged by less than a half, due to the error in pressure where the density changes sharply. At the same time, our INDSPH method is more stable in pressure calculation and can ensure the red phase is exactly half submerged. On the interface between the yellow and blue fluid phases, DFSPH produces a gap between phases because of the pressure error. The phases in the number density method are not fully separated. Using our method, clear interphase without a gap is presented between phases. This experiment shows the effect of two-phase fluid coupling and fluid-elastic coupling.

5.5 | Elastic deformation from tamponade

We further verify Young's modulus's influence on the elastic object's deformation. The experimental scenario is designed as the effect of silicone oil in the eye during vitrectomy combined with silicone oil tamponade surgery.

As shown in Figure 9, Figure 9a is the eye model reconstructed from the MRI images of a myopic patient, which has irregular shapes at the bottom. We use different materials with various Young's modulus in Figure 9b–d to examine how elasticity affects the result of silicone oil covering the surface of the cavity.

Comparative experiments are further conducted on differently shaped cavities. The top line of Figure 10 is the result of using the eyeball model, and the bottom line of Figure 10 is the result of using a regular sphere. Young's modulus of the transparent elastic object is 1 KPa, representing the fat tissue behind the eyeball. The white elastic object represents the sclera, which is the main structure that maintains the shape of the eyeball. Different deformation effects are obtained by changing Young's modulus of the sclera.

This experiment shows that our method can stably simulate the coupling of elastic objects with different Young's modulus. The experiment also proves that our method has particular potential in the application of medical visualization.
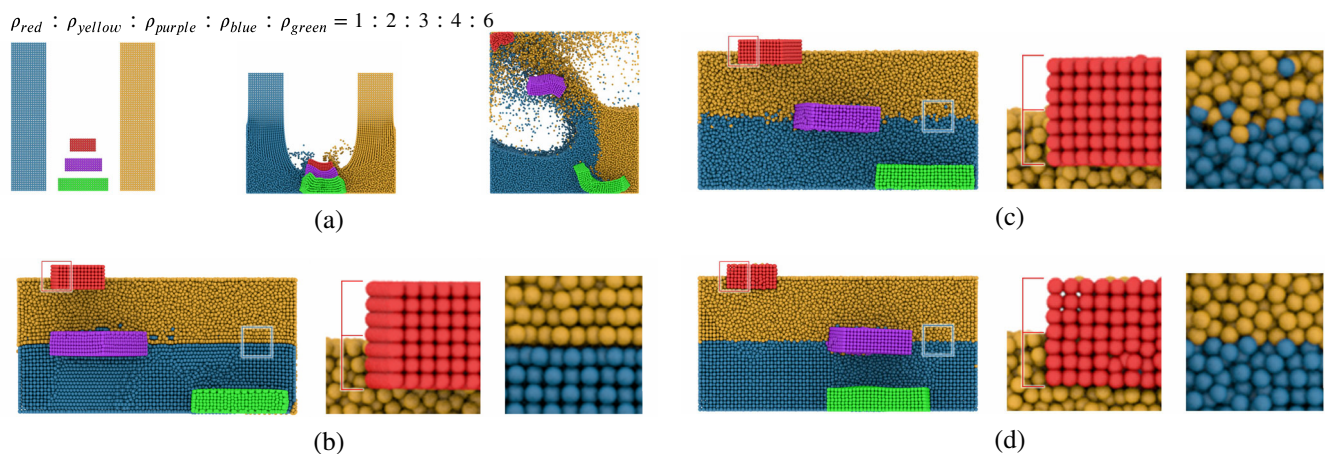

FIGURE 8 Coupling experiment between multiphase fluid and elastic objects. The fluid is displayed in cross-section. (a) Simulation process; (b-d) effects of different methods after reaching the steady state. (b) DFSPH; (c) number density; (d) INDSPH.
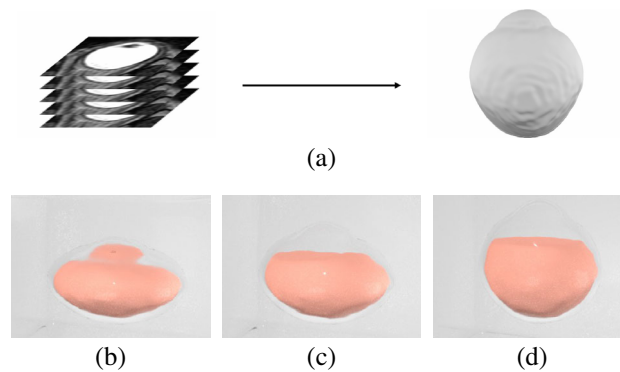
FIGURE 9 Simulation of silicone oil tamponade to the intraocular cavity. Biomechanical characteristics affect the result. (a) The eye model reconstructed from MRI images; (b) $E = 10$ KPa; (c) $E = 100$ KPa; (d) $E = 500$ KPa.
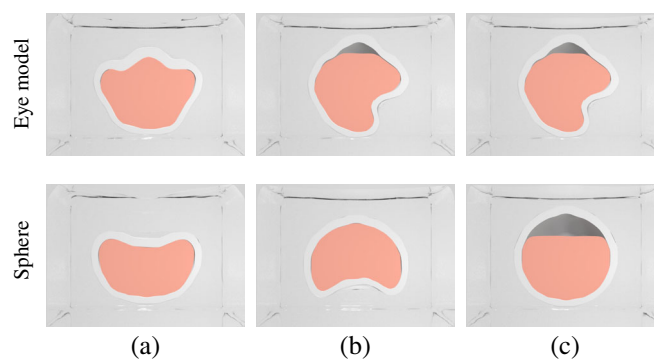

FIGURE 10 Filling effect of differently shaped intraocular cavities. (a) $E = 100$ KPa; (b) $E = 300$ KPa; (c) $E = 500$ KPa.

6 | CONCLUSIONS

This article presents an incompressible number density based SPH method that enables the implicit coupling of different phases with high density ratios. Based on the constraint of incompressibility of number density, we constructed a linear relationship between the divergence-free condition of the velocity field and the change rate of the local number density value. The proposed boundary handling scheme for INDSPH allows our solver to simulate fluid-fluid, fluid-rigid, fluid-elastic and rigid-elastic coupling simultaneously (Appendix S1). The number density incompressible solver can handle boundary coupling with a density ratio of up to 1:75 in our experiments and maintain a relatively low compression ratio compared to existing schemes.

However, some issues require to be further addressed. Currently, the INDSPH cannot handle a coupling with a higher density ratio (more than two orders of magnitude) to simulate a liquid–air interaction effect. This limitation comes from the drastic difference between liquid and air particles in the SPH Lagrangian system. We will study to find an extra mechanism to balance the mass difference and construct a more robust implicit coupling system, such as by applying different sizes of particles concerning the material density or using asynchronous time steps for different phases.

ORCID

Xiaokun Wang https://orcid.org/0000-0002-4449-591X
Yanrui Xu https://orcid.org/0000-0002-2154-1178

REFERENCES

1. Monaghan JJ. Smoothed particle hydrodynamics. Rep Prog Phys. 2005;68(8):1703.
2. Becker M, Teschner M. Weakly compressible SPH for free surface flows. Proceedings of the 2007 ACM SIGGRAPH/Eurographics Symposium on Computer Animation; 2007. p. 209–17.
3. Solenthaler B, Pajarola R. Density contrast SPH interfaces. Proceedings of the 2008 ACM SIGGRAPH/Eurographics Symposium on Computer Animation (SCA '08). Goslar: DEU, Eurographics Association; 2008. p. 211–8.
4. Solenthaler B, Pajarola R. Predictive-corrective incompressible SPH. Proceedings ACM SIGGRAPH 2009 papers; 2009. p. 1–6.
5. Ihmsen M, Cornelis J, Solenthaler B, Horvath C, Teschner M. Implicit incompressible SPH. IEEE Trans Vis Comput Graph. 2013;20(3):426–35.
6. Bender J, Koschier D. Divergence-free smoothed particle hydrodynamics. Proceedings of the 14th ACM SIGGRAPH/Eurographics symposium on computer animation; 2015. p. 147–55.
7. Peer A, Gissler C, Band S, Teschner M. An implicit SPH formulation for incompressible linearly elastic solids. Comput Graph Forum. 2018;37:135–48.
8. Bargteil AW, Shinar T, Kry PG. An introduction to physics-based animation. SIGGRAPH Asia 2020 Courses; 2020. p. 1–57.
9. Alduán I, Tena A, Otaduy MA. DYVERSO: a versatile multi-phase position-based fluids solution for VFX. Comput Graph Forum. 2017;36:32–44.
10. Li X, He X, Liu X, Zhang JJ, Liu B, Wu E. Multiphase interface tracking with fast semi-Lagrangian contouring. IEEE Trans Vis Comput Graph. 2015;22(8):1973–86.
11. Yang M, Ye J, Ding F, Zhang Y, Yan DM. A semi-explicit surface tracking mechanism for multi-phase immiscible liquids. IEEE Trans Vis Comput Graph. 2018;25(10):2873–85.
12. Teschner M, Heidelberger B, Muller M, Gross M. A versatile and robust model for geometrically complex deformable solids. Proceedings Computer Graphics International, 2004. IEEE; 2004. p. 312–9.
13. Koschier D, Bender J, Thuerey N. Robust eXtended finite elements for complex cutting of deformables. ACM Trans Graph. 2017;36(4):1–13.
14. Kugelstadt T, Koschier D, Bender J. Fast corotated FEM using operator splitting. Comput Graph Forum. 2018;37:149–60.
15. Jiang C, Gast T, Teran J. Anisotropic elastoplasticity for cloth, knit and hair frictional contact. ACM Trans Graph. 2017;36(4):1–14.
16. Becker M, Ihmsen M, Teschner M. Corotated SPH for deformable solids. Proceedings of the Fifth Eurographics Conference on Natural Phenomena; 2009. p. 27–34.
17. Ganzenmüller GC. An hourglass control algorithm for Lagrangian smooth particle hydrodynamics. Comput Methods Appl Mech Eng. 2015;286:87–106.
18. Kugelstadt T, Bender J, Fernández-Fernández JA, Jeske SR, Löschner F, Longva A. Fast corotated elastic SPH solids with implicit zero-energy mode control. Proc ACM Comput Graph Interact Tech. 2021;4(3):1–21.
19. Yang L, Li S, Hao A, Qin H. Realtime two-way coupling of meshless fluids and nonlinear FEM. Comput Graph Forum. 2012;31:2037–46.
20. Yan X, Jiang Y, Li C, Martin RR, Hu S. Multiphase SPH simulation for interactive fluids and solids. ACM Trans Graph. 2016;35(4):1–11.
21. Chen X, Li C, Cao G, Jiang Y, Hu S. A moving least square reproducing kernel particle method for unified multiphase continuum simulation. ACM Trans Graph. 2020;39(6):1–15. https://doi.org/10.1145/3414685.3417809
22. Fang Y, Qu Z, Li M, Zhang X, Zhu Y, Aanjaneya M, et al. IQ-MPM: an interface quadrature material point method for non-sticky strongly two-way coupled nonlinear solids and fluids. ACM Trans Graph. 2020;39(4):51–1.
23. Ott F, Schnetter E. A modified SPH approach for fluids with large density differences. arXiv preprint arXiv:physics/0303112, 2003.
24. Jiang Y, Li C, Deng S, Hu SM. A divergence-free mixture model for multiphase fluids. Comput Graph Forum. 2020;39:69–77.
25. Akinci N, Akinci G, Teschner M. Versatile surface tension and adhesion for SPH fluids. ACM Trans Graph. 2013;32(6):1–8.
26. Wang X, Ban X, Liu X, Zhang Y, Wang L. Effective reconstructing surfaces algorithm of anisotropic kernels orienting SPH fluids. J Comput-Aided Des Comput Graph. 2016;28:1497–505.

AUTHOR BIOGRAPHIES

Xiaokun Wang is an associate professor in School of Intelligence Science and Technology, University of Science and Technology Beijing, China. He received a Ph.D. degree in Computer Science and Technology from the University of Science and Technology Beijing, in 2017. He is currently working at the National Centre for Computer Animation at Bournemouth University funded by the EU's Horizon 2020 Marie Curie Individual Fellowship. His research interests include computer graphics, virtual reality, and human–computer interaction.

Tiancheng Wang is a postgraduate student at the School of Intelligence Science and Technology, University of Science and Technology Beijing. She received an undergraduate diploma in Shandong University of Science and Technology, in 2021. Her research field is computer graphics, especially physically-based fluid simulation.

Jiamin Wang is a PhD student at the School of Intelligence Science and Technology, University of Science and Technology Beijing. She received an undergraduate diploma in the University of Science and Technology Beijing, in 2021. Her research field is computer graphics, especially physically-based fluid simulation.

Yanrui Xu is a PhD student at the School of Intelligence Science and Technology, University of Science and Technology Beijing. He received his master's degree from the University of Science and Technology Beijing in 2020. His research interests include physical-based simulation and fluid animation.

Xiaojuan Ban is a professor at the School of Intelligence Science and Technology, University of Science and Technology Beijing. She is the leader of the Artificial Intelligence and 3D Visualization Group at University of Science and Technology Beijing, China. She received her master's degree in computer application and Ph.D. degree in control theory and control engineering from the University of Science and Technology Beijing. Her research interests include computer graphics, artificial intelligence, human–computer interaction, big data analysis, and 3D visualization.

Houbin Huang is a chief physician, professor and doctoral supervisor of Chinese PLA General Hospital Beijing. He specializes in the diagnosis and treatment of vitreoretinal diseases, neuro-ophthalmic diseases, especially complex and difficult fundus medical diseases, fundus imaging diagnosis and various laser treatments.

Zhihong Zhu is an attending physician at Hainan Hospital of Chinese PLA General Hospital. He is skilled in treating mechanical ocular trauma, cataract, and pterygium, and is good at the research of proteomics and bioinformatics.

Jian Chang is a professor in National Centre Computer Animation at Bournemouth University, United Kingdom. He received his Ph.D. degree in Computer Graphics from Bournemouth University, in 2007. His research interests include physics based modeling (deformation & fluid), motion synthesis, virtual reality (surgery simulation), and novel HCI (eye tracking, gesture control and haptic).

Jian Jun Zhang is a professor and director of the UK National Centre for Computer Animation Research at Bournemouth University. His research interests include 3D computer animation, virtual human modeling, virtual reality, and physics-based simulation.

SUPPORTING INFORMATION
Additional supporting information can be found online in the Supporting Information section at the end of this article.